PAPER

Check for updates

A ratiometric luminescence nanoprobe based on layered terbium hydroxide nanosheets for quantitative detection of an anthrax biomarker†

Jinyan Li,[ab] Qingyang Gu, [iD] *[ab] Hui Heng,[ab] Ziwei Wang,[ab] Haibo Jin[ab] and Jing He [iD] [c]

A novel ratiometric luminescence nanoprobe based on layered terbium hydroxide (LTbH) nanosheets was constructed for quantitative detection of dipicolinic acid (DPA), which was an anthrax biomarker. The LTbH nanosheets can be obtained by the exfoliation of the dodecyl sulfate (SDS) intercalated LTbH in formamide (FM). Upon the addition of DPA, the intrinsic green luminescence of Tb^{3+} can be sensitized due to the antenna effect. The luminescence intensity of FM at 332 nm as a reference remained almost constant, leading to ratiometric luminescence response toward DPA. The prepared luminescence nanoprobe was able to detect DPA with a linear relationship in the wide range of 1–100 μM, and the detection limit was 36.67 nM. In addition, the probe showed high selectivity and sensitivity for the detection of DPA as an anthrax biomarker and can be applied in actual tap water samples.

1. Introduction

Anthracnosis is a zoonotic, severe infectious disease caused by *Bacillus anthrax*, in which spores may be transmitted by food, water and air.[1–7] The inhalation of 10^4 *Bacillus anthracis* spores is deadly without treatment within 24–48 hours.[8–10] Anthrax has a microstructure that is highly resistant to extreme environments and can resist environments such as high temperature and high pressure, drought, ultraviolet irradiation, chemical disinfectants, strong acids and alkalis.[11–13] Thus, rapid and sensitive detection of *Bacillus anthrax* is critical for preventing and controlling anthrax disease and bioterrorism. Pyridine-2,6 dicarboxylic acid (DPA) is a major constituent of anthrax spores having a 5–15% dry mass ratio in the spores,[3,6,8,11,12,14] which is not present in other natural and synthetic materials.[15] As a result, DPA is an ideal biomarker for anthrax spores. Currently, several analytical methods are reported for the detection of DPA, such as high performance-liquid chromatography (HPLC),[16] polymerase chain reaction (PCR),[17] surface-enhanced Raman spectroscopy (SERS)[18] and quantitative fluorescence (FL) methods.[2,3] Among them, the FL technology for DPA

detection is increasingly favored by researchers for its outstanding advantages such as high sensitivity, rapid response time, and simplicity.[3] However, most of the currently reported DPA detection methods cannot simultaneously achieve high sensitivity and a wide linear range for DPA detection.[3,5,6,8] Therefore, it is very necessary to construct a new detection system for simple, fast, sensitive, and wide-range detection of DPA.

Lanthanide ions have been explored as excellent fluorescence probe materials due to their unique spectral properties, long fluorescence life, large stokes shifts, and sharp linear-like emission band caused by the parity-forbidden f–f transition.[3,8,19–21] DPA can transfer energy to lanthanide ions, thus the sensitized lanthanide ions can exhibit characteristic luminescence emission through the antenna effect.[21–23] Extensive work has been done on lanthanide ion modified carbon dots or quantum dots for the detection of DPA.[1–3,6,8]

Layered rare-earth hydroxide (LRH) is an anionic inorganic layered material,[21] which is composed of positively charged layers and negatively charged interlayers of anions.[20,24–26] Due to its rich interlayer chemical properties such as intercalation and ion exchange, it is widely used in the fields of adsorbent, catalysts and photochemical materials.[24,27] The general formula of LRH is $[RE_2(OH)_5(H_2O)n][A^{m-}]_{1/m}$ (RE = rare-earth ions, A^{m-} = anions).[24–26,28] Delaminated LRH nanosheets would be a very important class of functional 2D nanoscale materials,[20,29] which can be expanded by inserting organic or inorganic ions and further delaminated into monolayer nanosheets.[20] Investigations have found that

[a] *College of New Materials and Chemical Engineering, Beijing Institute of Petrochemical Technology, Beijing 102617, China. E-mail: guqingyang@bipt.edu.cn*
[b] *Beijing Key Laboratory of Fuels Cleaning and Advanced Catalytic Emission Reduction Technology, Beijing 102617, China*
[c] *State Key Laboratory of Chemical Resource Engineering, Beijing University of Chemical Technology, Beijing 100029, China*
† Electronic supplementary information (ESI) available. See DOI: 10.1039/d1sd00027f

intercalating surfactant ions such as dodecyl sulfate (SDS) into the interlayer can facilitate the exfoliation and that formamide (FM) is an excellent delaminating reagent.[20,30] Single luminescence probes based on Tb^{3+} doped nanosheets have been applied in the detection of DPA,[31] but the luminescence intensity based on lanthanide ions always suffers from the interference of instrumental factors or microenvironments. Ratiometric luminescence probes are highly attractive due to their self-calibration ability, which can reduce the interference. In this work, a luminescence nanoprobe, LNP(Tb), was constructed for quantitative luminescence detection of DPA through the intercalation and exfoliation of layered terbium hydroxide (LTbH). It's worth noting that LNP(Tb) served as a probe because the luminescence intensity of FM remains unchanged as a reference, while the Tb^{3+} ions can exhibit enhanced sharp luminescence emission upon the sensitization of DPA, enabling ratiometric DPA detection with a linear response in the nanomolar concentration range.

2. Experimental

2.1 Preparation of the Cl–LTbH precursor

A Cl–LTbH precursor was synthesized by a hydrothermal method as previously reported.[20,32] An aqueous solution containing $TbCl_3 \cdot 6H_2O$ (1 mmol), hexamethylenetetramine (HMT) (1 mmol), NaCl (13 mmol), and deionized water (80 ml) was heated at 90 °C for 12 h in a Teflon-lined autoclave. After the product was filtered, washed, and vacuum-dried (40 °C for 12 h), a Cl–LTbH precursor was obtained.

2.2 Preparation of the SDS–LTbH composite

The intercalation of SDS into LTbH was carried out by an ion-exchange reaction.[20] First, 1.26 mmol SDS was added to deionized water to form aqueous solutions. Then the Cl–LTbH powder (0.42 mmol) was dispersed into the above solutions. Finally, the reaction was conducted at 70 °C for 48 h in a Teflon-lined autoclave to give the precipitates, followed by filtration, washing, and vacuum drying. An SDS–LTbH composite was obtained.

2.3 Exfoliation of the SDS–LTbH composite

SDS–LTbH (40 mg) was dispersed into formamide (50 mL), and the resulting colloidal suspension was heated at 40 °C for 3 days without agitation. The Tyndall effect can be observed, as shown in Fig. 1(D). The prepared luminescence nanoprobe was denoted as LNP(Tb).

2.4 DPA detection by LNP(Tb)

2.0 mL of fresh LNP(Tb) solutions were mixed with 1.0 mL of fresh DPA solutions with different concentrations (0–100 μM). Next, after shaking vigorously for 10 seconds at room temperature, the corresponding luminescence data were measured using a fluorescence spectrophotometer at an excitation wavelength of 285 nm. In particular, all
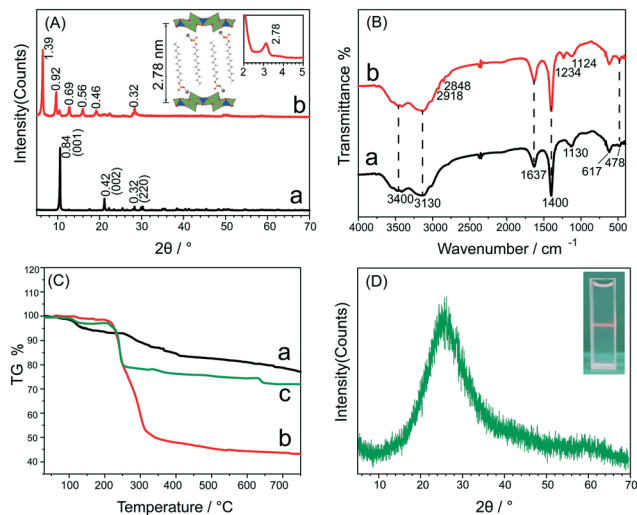

Fig. 1 (A) XRD patterns of the precursor Cl–LTbH (a) and the composite SDS–LTbH (b). (B) FT-IR spectra of the precursor Cl–LTbH (a) and the composite SDS–LTbH (b). (C) TG curves of the precursor Cl–LTbH (a), SDS (b) and the composite SDS–LTbH (c). (D) XRD pattern and the clear Tyndall light scattering of SDS–LTbH colloids.

measurements were carried out in triplicate to measure precision. Selectivity and ion interference experiments were carried out using the same method and concentration (30 μM).

2.5 Characterization

X-ray diffraction analysis (XRD) was carried out using a Shimadzu7000 X-ray diffractometer equipped with a Cu-Kα tube and an Al filter (k = 0.1542 nm) generated at 30 mA and 40 kV in a 2θ range from 5 to 70° at a scanning rate of 4° min^{-1}. For the small-degree measurements, XRD patterns were obtained in the 2θ range from 2 to 5°. Fourier transform infrared (FT-IR) spectra were recorded with a VERTEX70 spectrometer. The wavenumber range was set from 4000 to 400 cm^{-1}. The thermal decomposition behavior was measured in flowing air with a TGA HCT-1 thermal analyzer at a heating rate of 10 °C min from 30 to 750 °C. The morphologies of the LRH precursor and composite were observed using a field-emission scanning electron microscope (FESEM, Hitachi S-4800 microscope), while energy dispersive X-ray spectroscopy (EDS) mapping was performed on Hitachi S-8010 and Bruker XF lash 6160 instruments. The fluorescence lifetimes of samples were recorded with an Edinburgh FS5 spectrofluorimeter. Luminescence spectra were obtained on a Hitachi F-4500 spectrofluorimeter. The ex/em slit was 5 nm/5 nm, the light source was a xenon lamp, and the voltage was 700 V.

3. Results and discussion

3.1 Characterization of the layered structure

The XRD patterns of the Cl–LTbH precursor and SDS–LTbH composite are shown in Fig. 1(A). Fig. 1(A)-a shows a series of

strong (00*l*) reflections and a basal spacing (d_{basal}) of 0.84 nm, and the results for Cl–LTbH are consistent with the literature.[32] The sharp and symmetric diffractions suggest the formation of well-crystallized layered compounds.[24,33] For SDS–LTbH (Fig. 1(A)-b), a series of sharp and symmetric basal (00*l*) reflections are observed at 2.78, 1.39, 0.92, 0.69 and 0.56 nm with a basal spacing (d_{basal}) of 2.78 nm, indicating the well-ordered hydroxide layers.[20] The difference in the characteristic peaks of the LRH composite and the precursor results from the substitution of SDS anions for Cl⁻ in the interlayer of LTbH. According to previous reports, the thickness of the LRH layer is 0.65 nm[20,28,34] and the length of SDS is 1.82 nm,[20] and an interlayer spacing of 2.13 nm (= 2.78 nm–0.65 nm) suggests an alternating antiparallel monolayer arrangement of SDS vertical to the layer, as shown in Fig. 1(A).

The FT-IR spectra of the Cl–LTbH precursor and the SDS–LTbH composite are shown in Fig. 1(B). The bands at 3400 cm⁻¹ and 3130 cm⁻¹ belong to the stretching vibration absorptions of interlayer –OH and interlayer H_2O. The vibration absorption bands at 2918 and 2848 cm⁻¹ are the anti-symmetric and symmetric stretching vibrations in the alkyl chain of SDS, respectively.[20] The band at 1637 cm⁻¹ indicates the presence of H_2O molecules as bending vibration.[24,25] The band at 1400 cm⁻¹ can be assigned to the vibrations of the deprotonated C–H group. The absorption band at 1234 cm⁻¹ is the anti-vibration form of –OSO_3^-.[20] The bands at 1130 and 1124 cm⁻¹ are ascribed to the C–OH stretching vibrations.[35,36] The band at around 617 cm⁻¹ ascribed to the Tb–O vibrations also verify the formation of the layered composites.[24,25,28]

Fig. 1(C) shows the TG results for the precursor, organics, and composite. The weight loss of the composite (Fig. 1(C)-c) is much higher than that of Cl–LTbH (Fig. 1(C)-a) but lower than that of SDS (Fig. 1(C)-b), indicating that the composite has a good thermostability.

The XRD pattern of the SDS–LTbH colloids is shown in Fig. 1(D). There are no sharp basal reflections but with a halo in the 2θ range of 20–30°, which is due to the scattering of liquid formamide.[20] The XRD result verifies that the composite has been delaminated.

The morphologies of the synthesized samples are depicted in Fig. 2 *via* SEM observations, which shows a plate-like morphology with a rough surface. It can also be seen that the composites are composed of microcrystalline particles.[33] Cl–LTbH (Fig. 2(a)) mainly crystallizes into elongated hexahedral platelets, and some grow into columnar or flower-like aggregates, which are observed in previous studies.[24,28,33] SDS–LTbH (Fig. 2(b)) keeps the morphology of the Cl-LTbH precursor. A similar morphology between Cl-LTbH and SDS–LTbH reveals topological intercalation during the ion exchange progress.[27] The elemental mapping images and EDS results in the precursor Cl–LTbH and the SDS–LTbH composite are displayed in Fig. 2, which show the presence of different layer elements and the interlayer organic species. The relative brightness of the elements represents their corresponding content.

3.2 Luminescence properties of FM and LNP(Tb)

As shown in Fig. 3, the excitation spectrum of LNP(Tb) (Fig. 3(c)) was explored at an emission wavelength of 332 nm, and the emission spectrum of FM (Fig. 3(a)) and LNP(Tb) (Fig. 3(b)) was explored at an excitation wavelength of 285 nm, respectively. The emission at 332 nm belongs to FM, which acts as a reference in the detection. There exist weak Tb^{3+} characteristic emissions and a strong double frequency scattering peak (570 nm).

3.3 The detection of DPA

A quantitative luminescence study was conducted to evaluate the sensitivity of the ratiometric luminescence nanoprobe for DPA. Fig. 4(A) shows the luminescence response (λ_{ex} = 285 nm) of the nanoprobe when introducing different concentrations of DPA into the system. The emission spectrum of the nanoprobe without DPA was dominated by FM, with the major emission peak at 332 nm. Due to the antenna effect,[22,23] efficient energy transfers from DPA to Tb^{3+} ions, and the addition of a small amount of aqueous DPA solution enhances the emission intensity of Tb^{3+} ions. The emission peaks at 490, 544, 582, and 619 nm are attributed to the characteristic transitions of Tb^{3+} ions, from
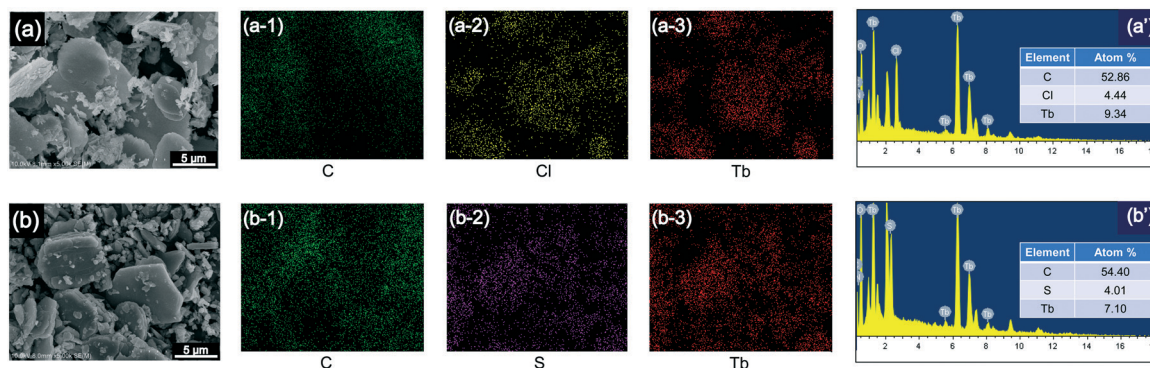

Fig. 2 SEM images of Cl–LTbH (a) and SDS-LTbH (b) and their corresponding elemental distribution mapping images ((a-1)–(a-3) and (b-1)–(b-3)) and related EDS results (a' and b').
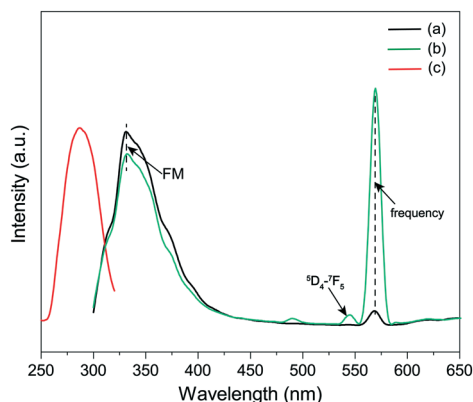
Fig. 3 Emission spectrum of FM (λ_{ex} = 285 nm) (a). Emission spectrum of LNP(Tb) (λ_{ex} = 285 nm) (b). Excitation spectrum of LNP(Tb) (λ_{em} = 332 nm) (c).

the $^5D_4$ energy level to ^7F_J multiplets (J = 6, 5, 4, and 3), respectively.[5,6,8,20] The maximum emission peak at 544 nm is narrow and sharp, thus resulting in excellent ratiometric measurements of DPA concentration.[8] The FL intensity of Tb^{3+} increases with the DPA concentration, especially for the emission at 544 nm. Furthermore, the FL intensity of FM at 332 nm remains constant with the addition of DPA, which can act as a ratiometric luminescence nanoprobe to detect DPA. According to Fig. 4(B), the FL intensity ratio (I_{544}/I_{332}) of LNP(Tb) is proportional to the concentration of DPA in the range of 1–100 μM and exhibits a strong linear relationship
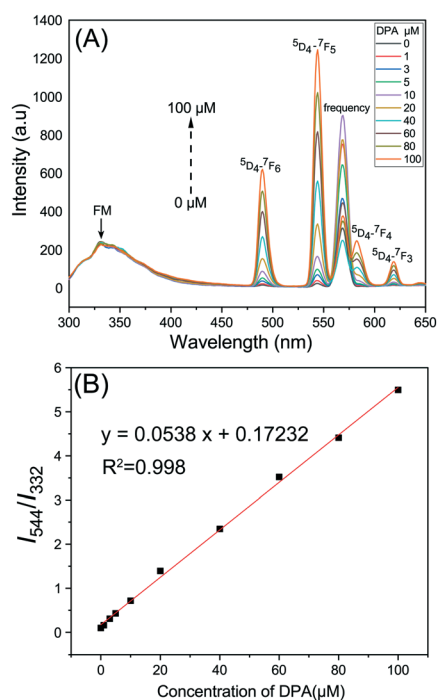
of R^2 = 0.998. The limit of detection (LOD) was determined to be 36.67 nM (LOD = $3S_b/m$, m is the slope of the calibration curve and S_b is the standard deviation of the blank), which is three orders of magnitude lower than an infectious dosage of the Bacillus thoracic spores (6×10^{-5} M required).[8,37] A comparison with a previously reported lanthanide based probe is shown in Table S1,† which shows that the probe has a relatively low detection limit and a wider detection range.

3.4 Interference detection

To study the selectivity of the system as a luminescence nanoprobe for DPA detection, the LNP(Tb) responses toward various potentially interfering substances are investigated, including aromatic carboxylic acids, amino acids and common biorelevant ions that are either structurally related to or can potentially be present in many bacterial spores along with DPA.[8]

As shown in Fig. 5, the selected interfering substances include glutamic (Glu), glycine (Gly), aspartic (Asp), phenylalanine (Phe), formic (FA), benzoic (BA), m-phthalic (m-PA) and m-toluic (m-TA) acid, which can coordinate with Tb^{3+} ions. In addition, common biorelevant ions (Cl^-, K^+, Fe^{3+}, Ca^{2+}, Mg^{2+}, Na^+, Cu^{2+}, Al^{3+}, and Ag^+) are tested. Remarkably, the FL intensity ratio (I_{544}/I_{332}) of the nanoprobe is almost unchanged when the interfering substance is added alone. However, when DPA is added, the FL intensity ratio (I_{544}/I_{332}) of the nanoprobes is significantly enhanced. It can

Fig. 4 (A) Evolution of the luminescence spectra of LNP(Tb) on increasing the DPA concentration (λ_{ex} = 285 nm). (B) Linear relationship between the DPA concentration and the fluorescence ratio (I_{544}/I_{332}) of LNP(Tb) in the concentration range of 1–100 μM.
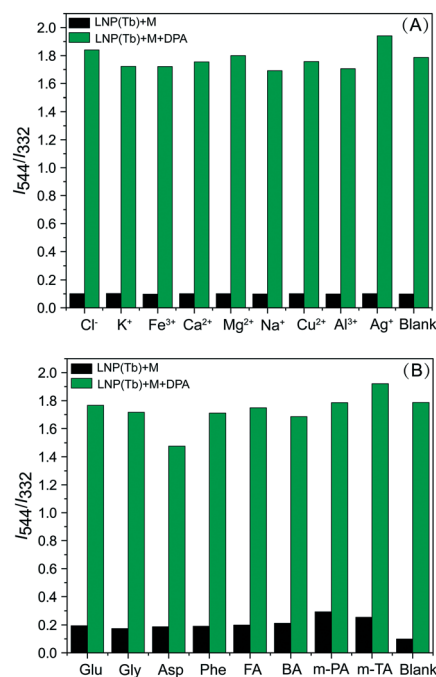

Fig. 5 Luminescence responses of LNP(Tb) toward different potentially interfering aromatic carboxylic acids or amino acids (A) and common biorelevant ions (B). The black bars represent an addition of 30 μM of the interfering acid or ion to LNP(Tb). The green bars represent a subsequent addition of 30 μM DPA to the solution (λ_{ex} = 285 nm).

be concluded that only DPA can induce significant luminescence enhancement at the same concentration, while the luminescence changes caused by other interference are negligible. Due to its excellent selectivity and anti-interference ability, the ratiometric sensing capability of this nanoprobe is not only useful for the quantitative determination of the DPA concentration but also not affected by intensity fluctuations due to instrumental or environmental factors. So this luminescence nanoprobe has great potential to be used for detecting DPA in complex samples.

3.5 Sensing applications in tap water

The usefulness of LNP(Tb) was evaluated by adding different concentrations of DPA to the tap water samples. As listed in Table 1, the experimental results show a good recovery rate and small relative standard deviation (RSD), and the recoveries of DPA are in the range of 96.65–101.79% with an RSD of 0.13–1.91% for tap water samples. This indicates that most of the results are accurate and reliable. As a result, the prepared LNP(Tb) can detect DPA in tap water samples accurately.

3.6 Fluorescence lifetimes of LNP(Tb)

As shown in Fig. 6, to further explore the antenna effect behavior between DPA and Tb^{3+}, fluorescence lifetime is measured at an excitation wavelength of 285 nm and collected at an emission wavelength of 544 nm. The measurement samples are the LNP(Tb) with different concentrations of DPA (0 μM and 30 μM). The logarithmic decay graphs are fitted with the single-exponential equation $I(t) = I_0 \exp(-t/\tau)$, where $I(t)$ is the fluorescence intensity dependent on time, I_0 is the fluorescence intensity at time zero, and τ is the lifetime.[27] LNP(Tb) with a concentration of 30 μM DPA (τ = 0.85 s) shows a longer fluorescence lifetime than LNP(Tb) without DPA (τ = 0.69 s). The results can be attributed to the antenna effect between DPA and Tb^{3+}, which enhances the luminescence of Tb^{3+} through energy transfer.

3.7 Luminescence mechanism analysis

Normally, the sensitization luminescence effect needs an effective energy transfer from the activators to the acceptors,[33,34] which means a perfect fit of the energy gap between the excited state energy levels of Tb^{3+} and the triplet state energy levels of the organics. If the energy difference is too large, then the probability of electron conversion will be little, thus decreasing the chance of transition. If the energy difference is too small, inverse or mutual transition may
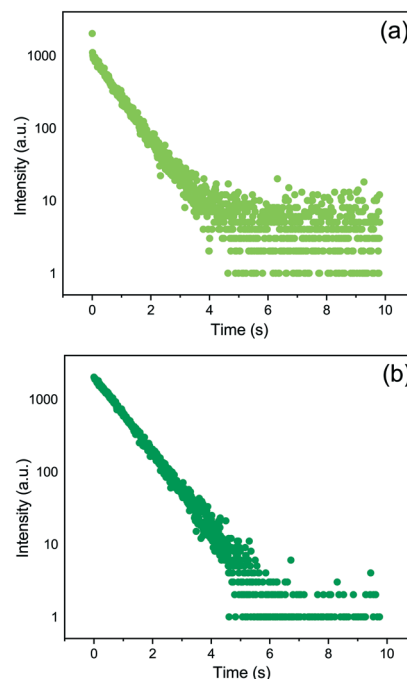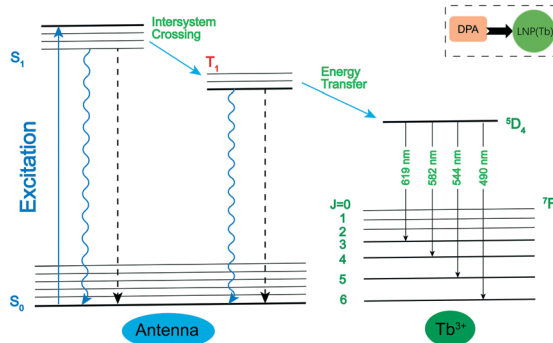

Fig. 6 Photoluminescence decay curves of LNP(Tb) without DPA (a) and with 30 μM DPA (b) (excited at 285 nm and monitored at 544 nm).

occur, while most of the energy would be inactivated by vibration rather than luminescence.[33] An energy gap of 3500 cm^{-1} or higher is necessary to facilitate efficient and irreversible energy transfer.[23,33] As shown in Scheme 1, the mechanism of the energy transfer can be ascribed to the antenna effect: DPA is excited by energy (usually the ultraviolet light) and electrons generate the π–π transition. That is, electrons transfer from the ground state to an excited singlet state ($S_0 \rightarrow S_1$), then quickly transfer from excited singlet state to excited triplet state ($S_1 \rightarrow T_1$) via intersystem crossing. Next, DPA at T_1 transfer energy to the lowest excited state of Tb^{3+}, thus emitting the characteristic luminescence of Tb^{3+}.[38,39] The energy gap between the triplet energy level of DPA (25 510 cm^{-1}) and the $^5D_4$ level of Tb^{3+} (20 540 cm^{-1})[23] is 4970 cm^{-1}, which is an excellent effective energy transfer.

Table 1 Detection of DPA in real samples (n = 3) by the probe

Sample	Added (μM)	Found (μM)	Recovery (%)	RSD (%)
Tap water	5.0	4.83	96.65	1.07
	10.0	10.17	101.79	1.91
	20.0	20.21	101.08	0.13

Scheme 1 Schematic diagram of the antenna effect mechanism of Tb^{3+}.

As a result, DPA can sensitize Tb^{3+} luminescence effectively, which provides a viable method to detect DPA.

4. Conclusions

In summary, a ratiometric luminescence nanoprobe was prepared by a simple method for quantitative detection of DPA. The XRD and FT-IR results indicate that SDS is successfully intercalated into LTbH to form an SDS–LTbH composite. Based on the Tyndall effect and XRD pattern of the SDS–LTbH colloids, SDS–LTbH has been successfully delaminated into nanosheets in FM. In the concentration range of 1–100 μM, the DPA concentration is linearly proportional to the FL intensity of Tb^{3+} at 544 nm. However, the FL intensity of FM at 332 nm remains constant, thus enabling the ratiometric detection of DPA. In addition, the luminescence nanoprobe exhibits a highly selective and sensitive detection of DPA, with a detection limit of 36.67 nM and long-term photostability. It's worth noting that LNP(Tb) can also be applied to detect DPA in tap water samples with good recovery rates and small RSD. This work provides a novel and effective method for quantitative detection of an anthrax biomarker.

Conflicts of interest

There are no conflicts to declare.

Acknowledgements

Notes and references

1 H. Yang, F. Lu, X. Zhan, M. Tian, Z. Yuan and C. Lu, A Eu(3+)-inspired fluorescent carbon nanodot probe for the sensitive visualization of anthrax biomarker by integrating EDTA chelation, *Talanta*, 2020, **208**, 120368–120376.

2 X. Liu, D. Chen, C. Wang, N. Tian, Z. Li, Y. Zhang and Z. J. Ding, A turn-on luminescence probe for highly selective detection of an anthrax biomarker, *Luminescence*, 2020, **35**, 601–607.

3 J. Wang, D. Li, Y. Qiu, X. Liu, L. Huang, H. Wen and J. Hu, An europium functionalized carbon dot-based fluorescence test paper for visual and quantitative point-of-care testing of anthrax biomarker, *Talanta*, 2020, **220**, 121377–121384.

4 B. Ma, F. Zeng, F. Zheng and S. Wu, Fluorescent detection of an anthrax biomarker based on PVA film, *Analyst*, 2011, **136**, 3649–3655.

5 X. Zhang, W. Zhang, G. Li, Q. Liu, Y. Xu and X. Liu, A ratiometric fluorescent probe for determination of the

6 Y. Y. Ma, Z. J. Wang and D. J. Qian, Ratiometric fluorescence detection of anthrax biomarker based on terbium (III) functionalized graphitic carbon nitride nanosheets, *Talanta*, 2021, **230**, 122311–122319.

7 J. Kim, H. Kim, N. Lee, T. Kim, H. Kim, T. Yu, I. Song, W. Moon and T. Hyeon, Multifunctional Uniform Nanoparticles Composed of a Magnetite Nanocrystal Core and a Mesoporous Silica Shell for Magnetic Resonance and Fluorescence Imaging and for Drug Delivery, *Angew. Chem., Int. Ed.*, 2008, **47**, 8438–8441.

8 H. Chen, Y. Xie, A. M. Kirillov, L. Liu, M. Yu, W. Liu and Y. Tang, A ratiometric fluorescent nanoprobe based on terbium functionalized carbon dots for highly sensitive detection of an anthrax biomarker, *Chem. Commun.*, 2015, **51**, 5036–5039.

9 K. Ai, B. Zhang and L. Lu, Europium-based fluorescence nanoparticle sensor for rapid and ultrasensitive detection of an anthrax biomarker, *Angew. Chem., Int. Ed.*, 2009, **48**, 304–308.

10 M. L. Cable, J. P. Kirby, K. Sorasaenee, H. Gray and A. Ponce, Bacterial Spore Detection by [Tb(3+)(macrocycle)(dipicolinate)] Luminescence, *J. Am. Chem. Soc.*, 2007, **129**, 1474–1475.

11 L. Meng, A. Bbc, H. Jia, B. Cml, F. Yuan and Z. Cheng, Anthrax biomarker: An ultrasensitive fluorescent ratiometry of dipicolinic acid by using terbium(III)-modified carbon dots, *Talanta*, 2019, **191**, 443–448.

12 N. Dey, D. Biswakarma and S. Bhattacharya, Metal Complex as an Optical Sensing Platform for Rapid Multimodal Recognition of a Pathogenic Biomarker in Real-Life Samples, *ACS Sustainable Chem. Eng.*, 2018, **7**, 569–577.

13 M. Yilmaz and H. A. Oktem, Eriochrome Black T-Eu^{3+} complex as a ratiometric colorimetric and fluorescent probe for the detection of dipicolinic acid, a biomarker of bacterial spores, *Anal. Chem.*, 2018, **90**, 4221–4225.

14 Y. Luo, L. Zhang, L. Zhang, B. Yu, Y. Wang and W. Zhang, Multiporous Terbium Phosphonate Coordination Polymers Microspheres as Fluorescent Probe for Trace Anthrax Biomarker Detection, *ACS Appl. Mater. Interfaces*, 2019, **11**, 15998–16005.

15 X. Bai, Y. Zeng, X. Zhou, X. Wang, A. G. Shen and J. Hu, Environmentally Safe Mercury(II) Ions Aided Zero-Background and Ultrasensitive SERS Detection of Dipicolinic Acid, *Anal. Chem.*, 2017, **89**, 10335–10342.

16 J. Fichtel, H. Sass and J. Rullkötter, Assessment of spore contamination in pepper by determination of dipicolinic acid with a highly sensitive HPLC approach, *Food Control*, 2008, **19**, 1006–1010.

17 K. M. Y. Yoon, Recent advances in rapid and ultrasensitive biosensors for infectious agents: lesson from Bacillus anthracis diagnostic sensors, *Analyst*, 2010, **135**, 1182–1190.

18 R. M. Jarvis and R. Goodacre, Discrimination of Bacteria Using Surface-Enhanced Raman Spectroscopy, *Anal. Chem.*, 2004, **76**, 40–47.

anthrax biomarker 2,6-pyridinedicarboxylic acid based on a terbium(III)- functionalized UIO-67 metal-organic framework, *Microchim. Acta*, 2020, **187**, 122–129.

19 R. Ju and Q. Gu, Biohybrid based on layered terbium hydroxide and applications as drug carrier and biological fluorescence probe, *Appl. Organomet. Chem.*, 2018, **32**, 3926–3934.

20 Y. Zhao, J. G. Li, M. Guo and X. Yang, Structural and photoluminescent investigation of LTbH/LEuH nanosheets and their color-tunable colloidal hybrids, *J. Mater. Chem. C*, 2013, **1**, 3584–3592.

21 C. Tan, Q. Wang and C. C. Zhang, Optical and electrochemical responses of an anthrax biomarker based on single-walled carbon nanotubes covalently loaded with terbium complexes, *Chem. Commun.*, 2011, **47**, 12521–12523.

22 M. C. Heffern, L. M. Matosziuk and T. J. Meade, Lanthanide probes for bioresponsive imaging, *Chem. Rev.*, 2014, **114**, 4496–4539.

23 Y. Zhou, X. Li, L. Zhang, Y. Guo and Z. Shi, 3-D silver(I)-lanthanide(III) heterometallic-organic frameworks constructed from 2,2′-bipyridine-3,3′-dicarboxylic acid: synthesis, structure, photoluminescence, and their remarkable thermostability, *Inorg. Chem.*, 2014, **53**, 3362–3370.

24 Q. Gu, J. Li, L. Ji, R. Ju, H. Jin and R. Zhang, Fabrication of novel bifunctional nanohybrid based on layered rare-earth hydroxide with magnetic and fluorescent properties, *Front. Mater. Sci.*, 2020, **14**, 488–496.

25 Q. Gu, Y. Wu and S. Yu, Organic-inorganic luminescent composites obtained by the intercalation of organic dyes into the layered rare-earth hydroxides, *Inorg. Chim. Acta*, 2019, **487**, 162–168.

26 Q. Gu, M. Yuan, S. Ma and G. Sun, Structures and photoluminescence properties of organic-inorganic hybrid materials based on layered rare-earth hydroxides, *J. Lumin.*, 2017, **192**, 1211–1219.

27 R. Guo, J. Li, L. Chen, Z. Yu, H. Yao, K. Shi, C. Li and S. Ma, SDC/OS-LDH composite for highly sensitive fluorescence detection of Fe(3+) at a much lower concentration, *Dalton Trans.*, 2020, **49**, 10413–10420.

28 Q. Gu, W. Chen, F. Duan and R. Ju, Fabrication of a nano-drug delivery system based on layered rare-earth hydroxides integrating drug-loading and fluorescence properties, *Dalton Trans.*, 2016, **45**, 12137–12143.

29 Q. Gu, F. Su, L. Ma, S. Ma, G. Sun and X. Yang, Intercalation of coumaric acids into layered rare-earth hydroxides: controllable structure and photoluminescence properties, *J. Mater. Chem. C*, 2015, **3**, 4742–4750.

30 L. Hu, R. Ma, T. Ozawa and T. Sasaki, Exfoliation of Layered Europium Hydroxide into Unilamellar Nanosheets, *Chem. – Asian J.*, 2010, **5**, 248–251.

31 B. Wang, J. Xia, G. Zhou, X. Li, M. Dai, D. Jiang and Q. Li, Tb(III)-doped nanosheets as a fluorescent probe for the detection of dipicolinic acid, *RSC Adv.*, 2020, **10**, 37500–37506.

32 F. Su, Q. Gu, S. Ma, G. Sun, X. Yang and L.-D. Zhao, Delaminated layered rare-earth hydroxide composites with ortho-coumaric acid: color-tunable luminescence and blue emission due to energy transfer, *J. Mater. Chem. C*, 2015, **3**, 7143–7152.

33 R. Guo, F. Su, H. Wang, Y. Guo, H. Yao, G. Huang, J. Li, Z. Liang, K. Shi and S. Ma, Luminescence Tuning of Layered Rare-Earth Hydroxides (LRHs, R = Tb, Y) Composites with 3-Hydroxy-2-naphthoic Acid and Application to the Fluorescent Detection of Al(3+), *Inorg. Chem.*, 2019, **58**, 4979–4988.

34 N. Chu, Y. Sun, Y. Zhao, X. Li and X. Yang, Intercalation of organic sensitisers into layered europium hydroxide and enhanced luminescence property, *Dalton Trans.*, 2012, **41**, 7409–7414.

35 M. Luo, S. Xu, Q. Gu, Z. Di, Q. Liu and Z. Zhao, Co-Al nanosheets derived from LDHs and their catalytic performance for syngas conversion, *J. Colloid Interface Sci.*, 2019, **538**, 440–448.

36 Y. Zhu, Y. Zhou, Z. Tao, M. He, Y. Wang, X. Yang and Y. Yong, Preparation and characterization of lactate-intercalated Co–Fe layered double hydroxides and exfoliated nanosheet film with low infrared emissivity, *Appl. Surf. Sci.*, 2012, **263**, 132–138.

37 P. M. Pellegrino, N. F. Fell, D. L. Rosen and J. B. Gillespie, Bacterial Endospore Detection Using Terbium Dipicolinate Photoluminescence in the Presence of Chemical and Biological Materials, *Anal. Chem.*, 1998, **70**, 1755–1760.

38 E. G. Moore, A. P. S. Samuel and K. N. Raymond, From Antenna to Assay: Lessons Learned in Lanthanide Luminescence, *Acc. Chem. Res.*, 2009, **42**, 542–552.

39 C. P. Montgomery, B. S. Murray, E. J. New, R. Pal and D. Parker, Cell-Penetrating Metal Complex Optical Probes: Targeted and Responsive Systems Based on Lanthanide Luminescence, *Acc. Chem. Res.*, 2009, **42**, 925–937.